

Supporting Information for

Closed-Loop Recycling of Spent $\text{Li}_{6.5}\text{La}_3\text{Zr}_{1.5}\text{Ta}_{0.5}\text{O}_{12}$: From Selective Lithium Recovery to High-Efficiency Sintering-Aid Preparation

*Yufan Zheng, Kexing Wan, Yuancheng Chen, Chuang Ji, Hongxiang Kuai, and Xunhui Xiong**

1. Experimental Section

Experimental Procedures

The spent SSBs used in this study were obtained from end-of-life batteries after cycle testing. To ensure safety, the batteries were first fully discharged in a 5% NaCl (w/v) solution for 24 h, followed by manual disassembly. The separated components were subsequently immersed in an ethanol solution to facilitate the detachment of the cathode and anode from the SSEs.

Selective Li Extraction of Spent LLZTO SSEs: Firstly, the SSEs were crushed into fine powder by ball milling using a planetary ball mill (QM-3SP2, Instrumentation Factory, Nanjing University) at 500 rpm for 6 h. The crushed powder was homogeneously mixed with a certain proportion of sulfur, $\text{Na}_2\text{S}_2\text{O}_3$ or $\text{Na}_2\text{S}_2\text{O}_8$. The mixed powder was placed in a tube furnace and heated to the specified temperature at a rate of $5\text{ }^\circ\text{C min}^{-1}$ under a N_2 atmosphere and maintained for a specific period of time. Once the roasting was accomplished, Li was selectively leached using deionized water as the leaching agent. After filtration, the Li-containing mother liquid was evaporated and concentrated, followed by the addition of sodium carbonate solution to precipitate Li. After filtration and drying, Li_2CO_3 was obtained.

Synthesis of SSE Sintering Aids: The Li extraction slag was annealed in a tube furnace at a heating rate of $5\text{ }^\circ\text{C per minute}$ in an air atmosphere. After natural cooling, the excessive La was separated using 0.01 M sulfuric acid. After filtration and drying, the SSE sintering aid LZTO was obtained.

Synthesis of Solid Electrolytes: Cubic phase $\text{Li}_{6.5}\text{La}_3\text{Zr}_{1.5}\text{Ta}_{0.5}\text{O}_{12}$ was synthesized by a solid-state approach. The starting materials, including $\text{LiOH}\cdot\text{H}_2\text{O}$, ZrO_2 , La_2O_3 , and Ta_2O_5 , were dried under vacuum at 60 °C and mixed in stoichiometric ratios. The mixture was ball milled with isopropanol for 12 h at 360 rpm. After drying, the mixture was sintered at 900 °C for 5 h. The prepared powder was further ball milled, with 2 wt% LZTO added to form LLZTO-LZTO, while another batch was directly labeled as LLZTO without LZTO addition. Finally, the powder was pressed into green body and sintered at 1240 °C for 0.5 h with a heating rate of 5 °C/min.

Analytical method

The metal composition and content in spent LLZTO SSEs and leach solution were determined using Inductively Coupled Plasma Optical Emission Spectroscopy (ICP-OES). To ensure the accuracy of the test results, each sample was measured in triplicate, and the average value of the measurements was used as the final result. The Relative Standard Deviation (RSD) of the obtained data was less than 3%. The leaching efficiency of Li was calculated based on the following formula:

$$\eta = \frac{c_i V}{m_0 w_i} * 100\%$$

Where m_0 is the mass of spent LLZTO powder taken, w_i is the mass percentage of element "i" in the leachate, c_i and V is the concentration and the volume of element "i" in the leachate, respectively.

Material characterization

The attention of Li was analyzed by Inductively Coupled Plasma Optical Emission Spectrometer (ICP-OES, Agilent 730, USA). XRD patterns were obtained by an X-ray diffractometer (Bruker D8 ADVANCE) with Cu $K\alpha$ radiation ($\lambda = 1.5405 \text{ \AA}$). The morphology analysis was carried out with a field-emission scanning electron microscope (SEM, sigma 300 vp, ZEISS). Surface compositions were investigated with X-ray photoelectron spectroscopy (XPS, American Thermo Fisher Scientific ESCALAB 250Xi). Thermogravimetric analysis/Differential scanning calorimetry (TG/DSC, METTLER TOLEDO) was employed to verify the phase transformation process. The size distribution of attrition-milled LZTO particles and ball-milled LLZTO

particles was determined using a laser particle size analyzer (Mastersizer 2000; Malvern). The densities of the sintered pellets were measured at room temperature (25 °C) using the Archimedes method with ethanol as the immersion medium and a Mettler–Toledo density measurement attachment. Techno-economic and life-cycle assessments of various processes were carried out using the EverBatt model and the greenhouse gases, regulated emissions, and energy use in transportation (GREET) model developed by Argonne National Laboratory.

Electrochemical measurements

The LLZTO and LLZTO-LZTO were grounded until 5000# sandpaper and polished for the preparation of cells. LiFePO_4 (LFP) cathodes and Li metal anodes were employed to assemble the solid-state batteries. The battery was cycled with a voltage range of 2.5~4.0 V at room temperature. Symmetric cells were assembled by uniformly attaching lithium metal to both sides of garnet particles.

2. Supplementary text

Supplementary text 1. Details of technoeconomic analysis (TEA).

In order to evaluate the economic potential of sulfidation roasting process for the recovery of spent solid electrolytes, TEA simulations of the entire recovery process were carried out to demonstrate the application of the process in practical production. The entire recycling process flow based on used garnet-based solid-state batteries was analyzed, including three main steps of pretreatment, lithium extraction by roasting and synthesis by secondary roasting. The feedstock ratios, reaction parameters (operating temperature, reaction time, etc.), and yields of the products used in the TEA process were determined with reference to the actual pilot scale.

The total cost of the process of recovering spent solid electrolytes by sulfidation roasting was calculated using specific samples as an example.

The economic potential of our proposed solid electrolyte recycling process is illustrated by the example of 1.825 tons of spent solid electrolyte per year. The details of the calculations, such as material ratios and reaction parameters, have been carefully chosen to match the actual experimental conditions of our laboratory-scale treatment of

solid electrolytes. Specifically, we have assumed a daily treatment rate of 5 kg day⁻¹ of spent solid electrolyte, resulting in an annual treatment rate of 1,825 tons of spent solid electrolyte. The annual running times for the equipment were determined based on their actual working time in preparation processes. The specific assumptions have been discussed in the following texts for cost calculations. The material flow with subdivided costs for the entire solid electrolyte recovery process was analyzed, which could provide some reference and guidance, and of course, the actual profit must be determined after a large-scale.

1. Capital cost. The total capital cost was regarded as encompassing the equipment purchase cost as well as other capital costs. Equipment life is assumed to be ten years for equipment purchase costs. Other capital costs were usually derived from equipment installation, process piping, instrumentation and controls, electrical systems, etc. These costs are challenging to determine as they rely on numerous factors, and certain approximations exist to estimate these costs as a percentage. To guarantee the accuracy of the outcomes, we have referred to the methods previously reported for calculating the capital costs. The other capital costs are 50% of the cost of the equipment.

(1) Equipment purchase cost:

= (\$1587 (planetary activator) + \$10534.12 (tube furnace) + \$140.45 (agitated tank) × 2) ÷ 10 = \$1240.20

(2) Other capital costs:

= \$12203.9 × 50% = \$6201.01

2. Operating costs. Operating costs were considered to include electricity, maintenance, labor, depreciation and other operating costs (e.g. administration, insurance, etc.). The selected tariff (0.0843 \$ kWh⁻¹) is based on the local electricity price in Guangzhou, China. Annual maintenance materials as 2.0% of total equipment cost. Labor costs are based on the average wage for manufacturing and related personnel in China in 2023 (data from the National Bureau of Statistics). Depreciation of 10% of capital costs. Administrative costs (administrative staff, office, sales network, etc.) account for 45.0% of labor costs. The premium is 1% of capital costs.

(1) Electricity:

$$= (1.5 \text{ kW} \times 3 \text{ h day}^{-1} + 7 \text{ kW} \times 12.5 \text{ h day}^{-1} + 0.02 \text{ kW} \times 2 \text{ h day}^{-1}) \times 365 \text{ day} \times 0.0843 \text{ \$ kWh}^{-1} = \$2616.64$$

(2) Maintenance:

$$= \$12402.02 \text{ (equipment purchase cost)} \times 2.0\% = \$248.04$$

(3) Labor:

$$= \$10599.15$$

(4) Depreciation:

$$= \$18603.03 \times 10\% = \$1860.3$$

(5) Other operating cost:

$$= \$10599.15 \times 45.0\% \text{ (administrative cost)} + \$18603.03 \times 1\% \text{ (premium)} = \$4955.65$$

3. Material costs. Prices for all starting chemicals and reagents are based on industrial grade purity reagents from local suppliers. The annual consumption of these chemicals is based on their daily use in laboratory-scale production.

(1) Sulfur:

$$= 165.15 \text{ \$ t}^{-1} \times 1.8 \text{ t} = \$297.27$$

(2) Sodium Carbonate:

$$= 238.77 \text{ \$ t}^{-1} \times 1.4 \text{ t} = \$323.59$$

(3) Oxalic acid:

$$= 431.47 \text{ \$ t}^{-1} \times 0.3 \text{ t} = \$129.44$$

(4) Ethanol:

$$= 780.05 \text{ \$ t}^{-1} \times 3.6 \text{ t} = \$2,808.18$$

(5) Other chemicals (sulfuric acid, argon, water):

$$= 36.51 \text{ \$ t}^{-1} \times 0.02 \text{ t} + 61.8 \text{ \$ t}^{-1} \times 0.002 \text{ t} + 0.48 \text{ \$ t}^{-1} \times 36.5 \text{ t} = \$19.48$$

4. Total cost.

$$\text{Total cost} = (\$1240.20 + \$6201.01) + (\$2616.64 + \$248.04 + \$10599.15 + \$1860.3 + \$4955.65) + (\$297.27 + \$323.59 + \$129.44 + \$19.48 + \$2,808.18) = \$31293.59$$

5. Income. The products of the spent solid electrolyte recycling process are Li_2CO_3 , La_2O_3 and $\text{La}_3\text{Zr}_{1.5}\text{Ta}_{0.5}\text{O}_{8.75}$, and income is estimated based on prices in China.

$$\text{Income} = 10361.45 \text{ \$ t}^{-1} \times 0.47 \text{ t} + 2505.29 \text{ \$ t}^{-1} \times 0.67 \text{ t} + 42205.5 \text{ \$ t}^{-1} \times 0.87 \text{ t} =$$

3. Supplementary Figures and Tables

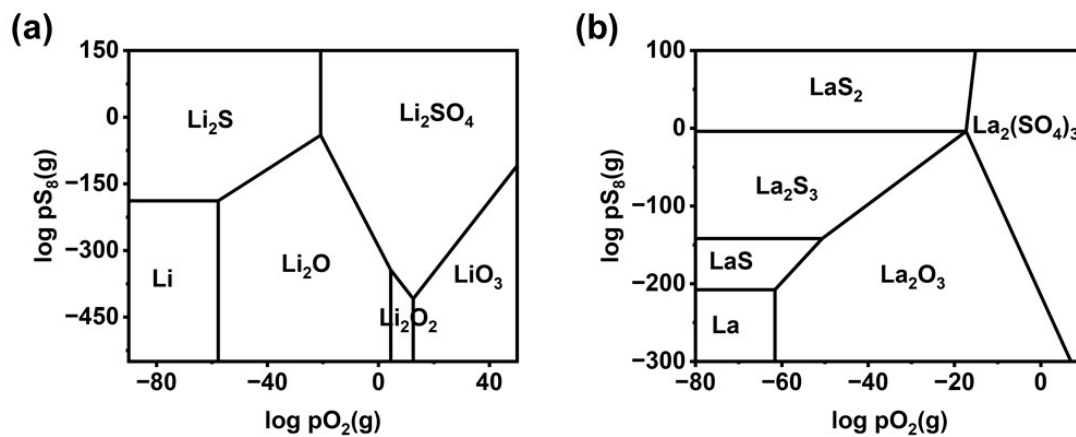


Figure S1. Predominance diagrams of (a) Li-S-O and (b) La-S-O system at 600 °C.

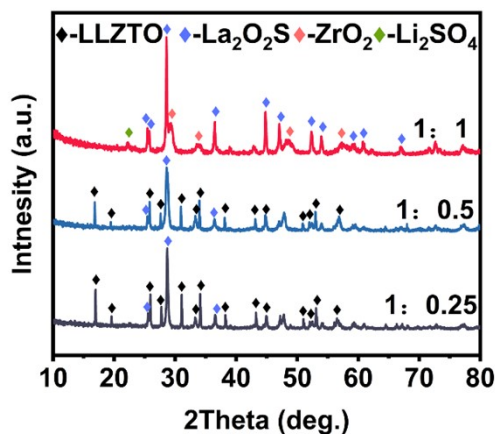


Figure S2. XRD patterns of the roasted products with different S/LLZTO mass ratios.

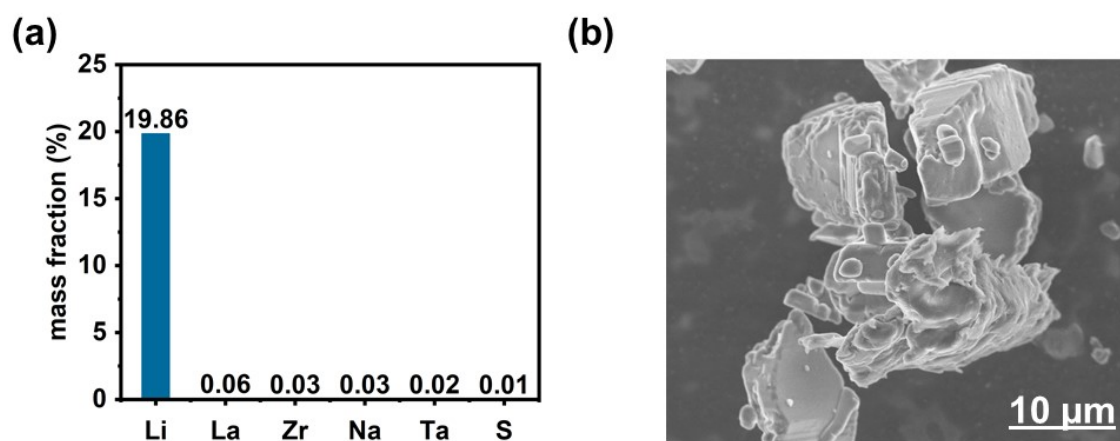


Figure S3. (a) Elemental mass fraction and (b) SEM image of the recycled Li_2CO_3 .

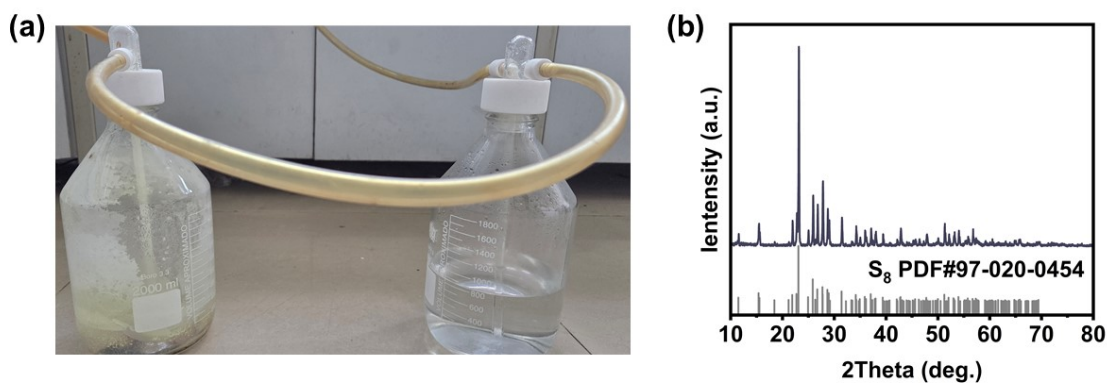


Figure S4. (a) Tail gas absorber and (b) XRD patterns of condensed sulfur powder.

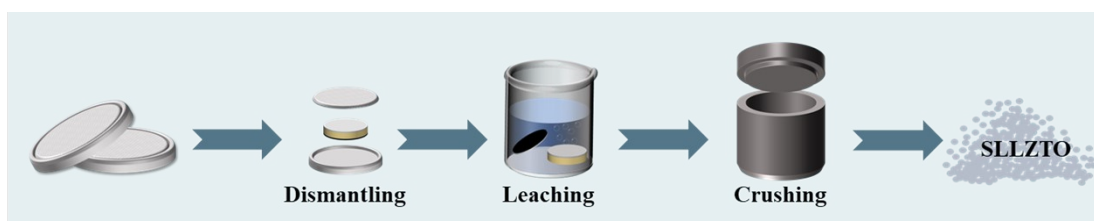


Figure S5. Pretreatment process for recycling spent garnet-based SSBs.

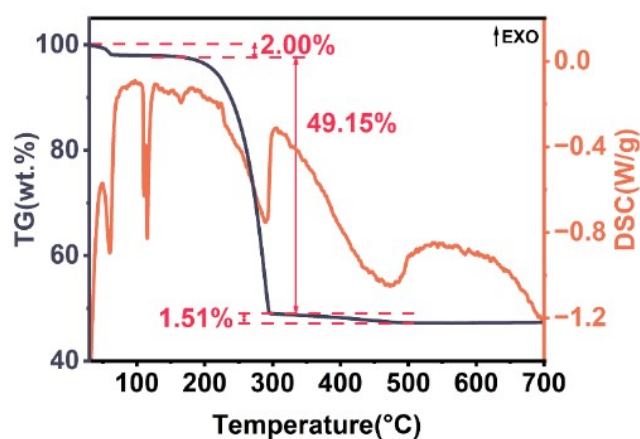


Figure S6. TG-DSC curves of sulfur - based phase transformation.

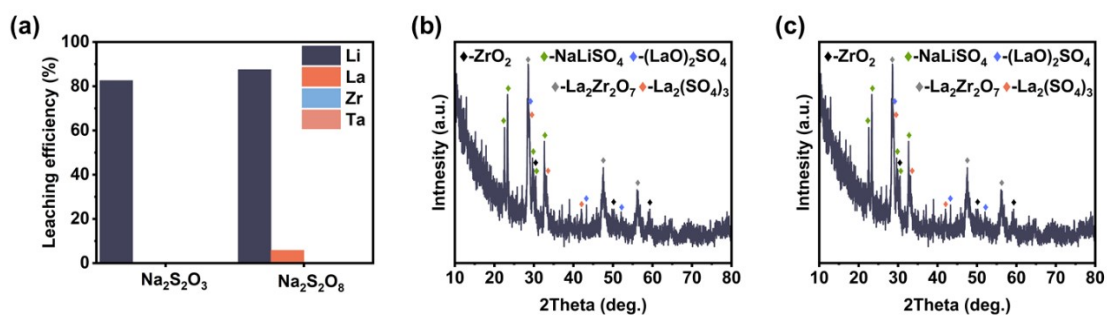


Figure S7. (a) Elemental leaching efficiency using different sulphurising agents. XRD pattern of the roasted products with (b) $\text{Na}_2\text{S}_2\text{O}_3$ and (c) $\text{Na}_2\text{S}_2\text{O}_8$.

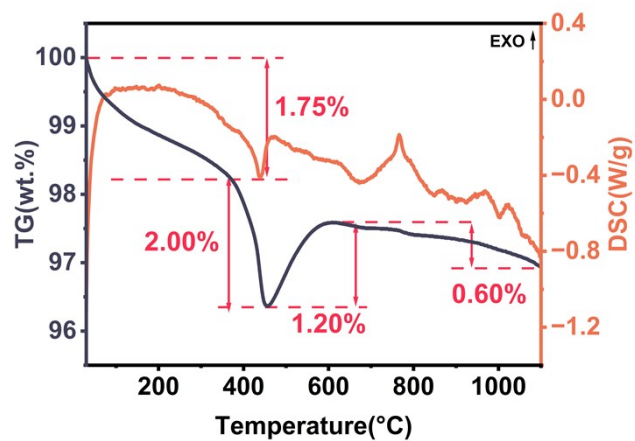


Figure S8. TG-DSC curves of second roasting.

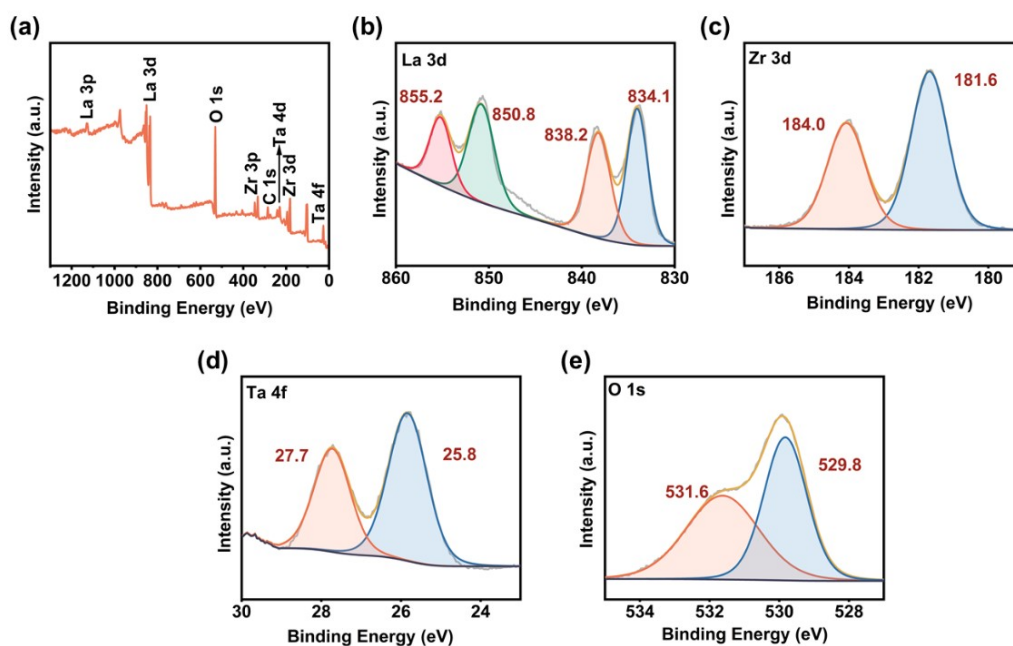


Figure S9. XPS survey spectrum of LZTO.

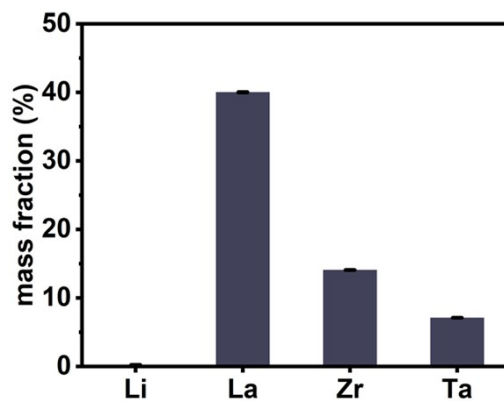


Figure S10. Elemental content of the LZTO.

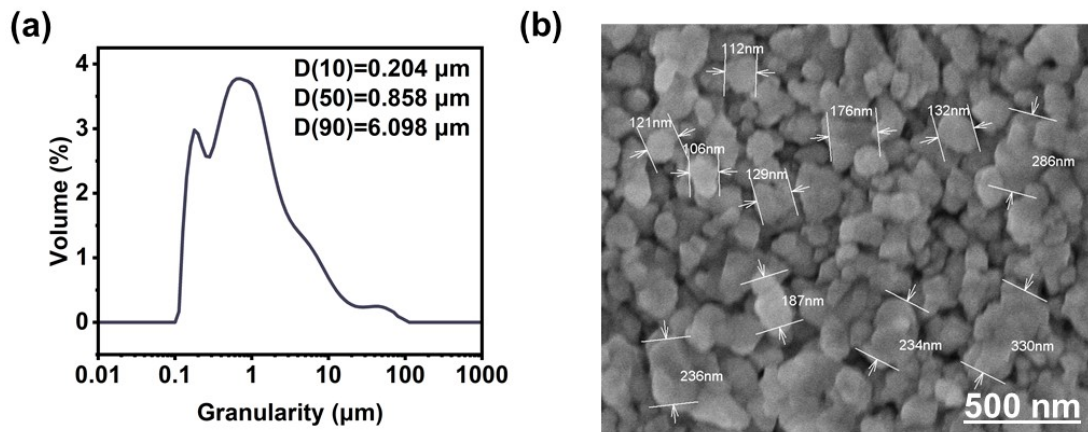


Figure S11. The particle size distribution (a) and SEM image (b) of LZTO.

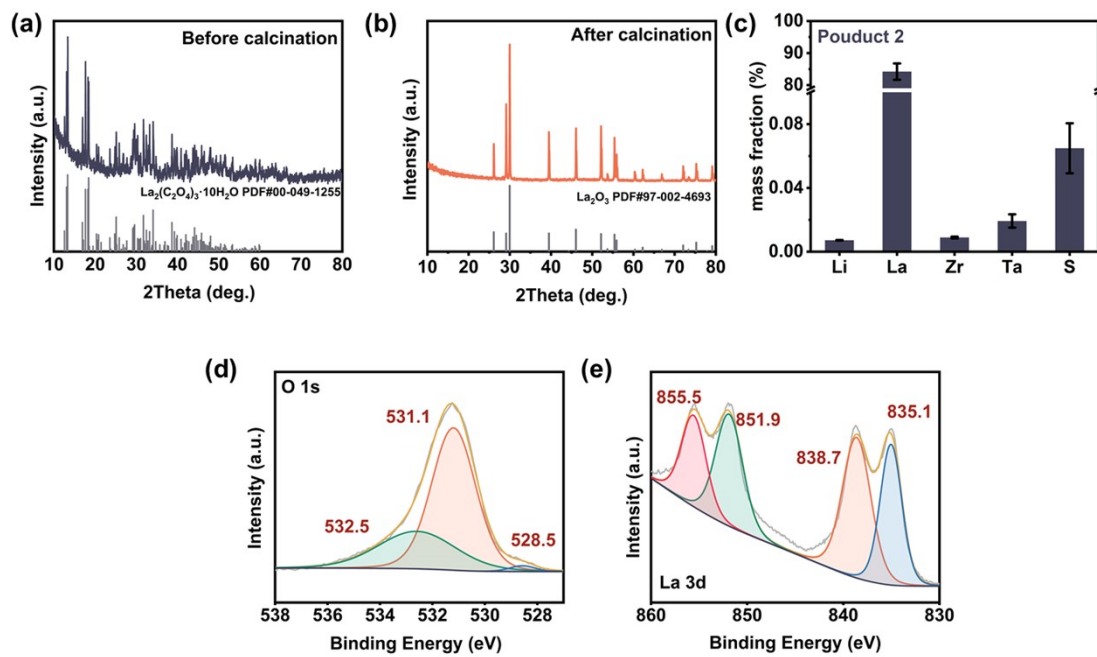


Figure S12. XRD patterns of La_2O_3 (a) before and (b) after calcination. (c) Elemental content and (d-e) XPS mapping of La_2O_3 .

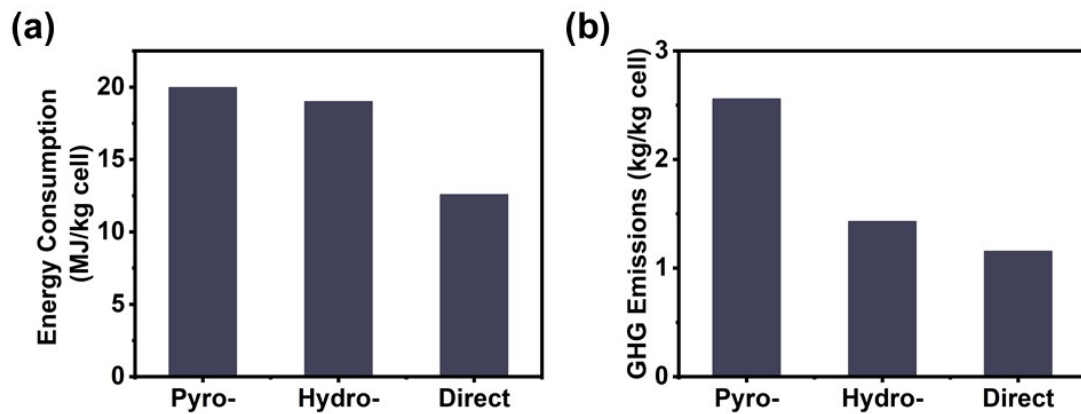


Figure S13. Comparison of (a) energy consumption and (b) GHG emissions of

different recycling processes for spent LIBs.

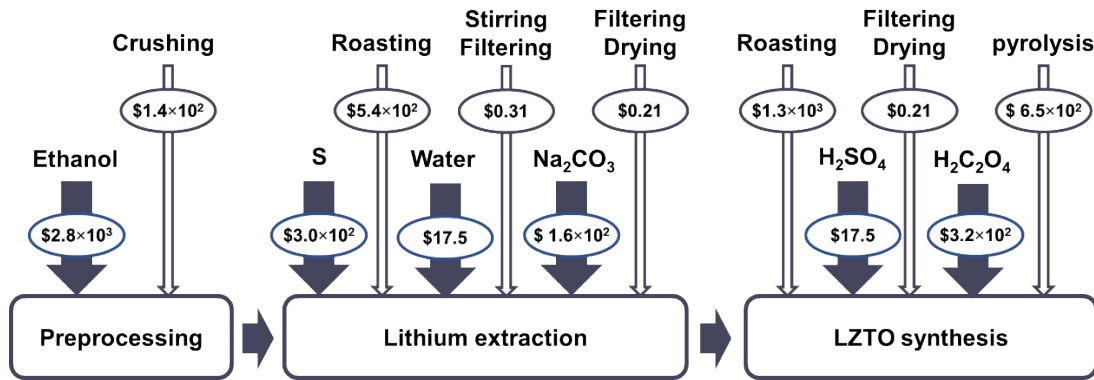


Figure S14. Material flow analysis of the specific example of selective extraction of sulfur-based phase transformation.

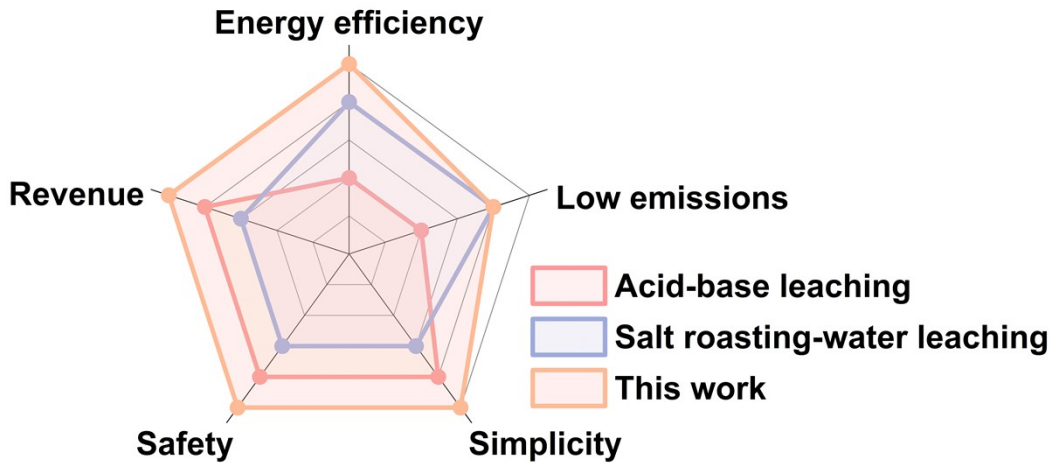


Figure S15. Comprehensive comparison of different battery recycling technologies.

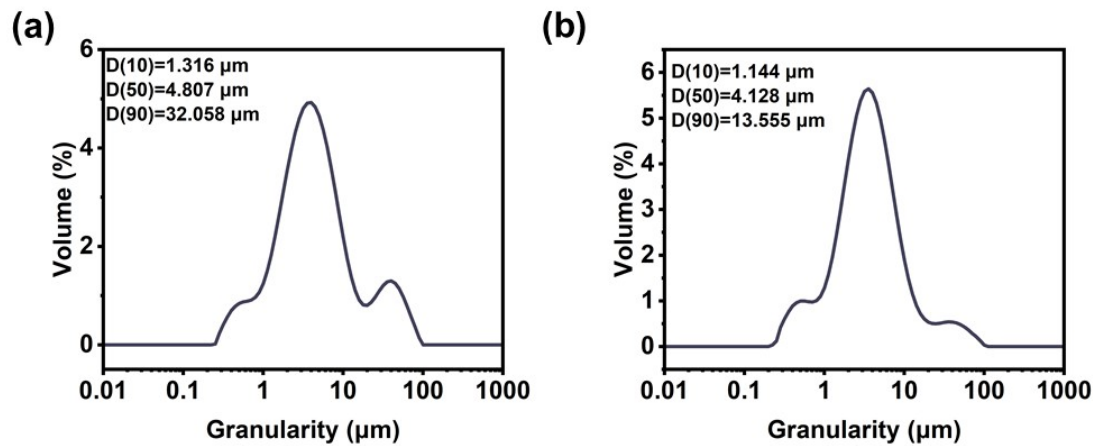


Figure S16. The particle size distribution of (a) LLZTO and (b) LLZTO-LZTO.

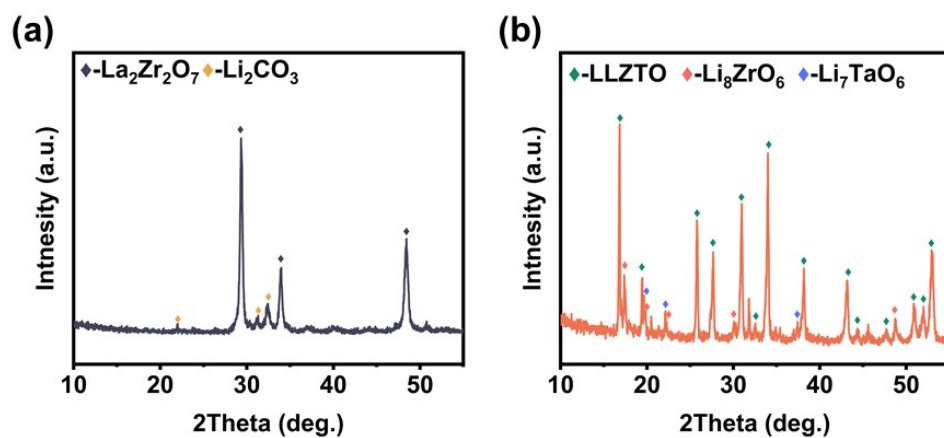


Figure S17. XRD patterns for LiOH·H₂O-LZTO pellets (a) before and (b) after sintered at 1240 °C for 0.5 h.

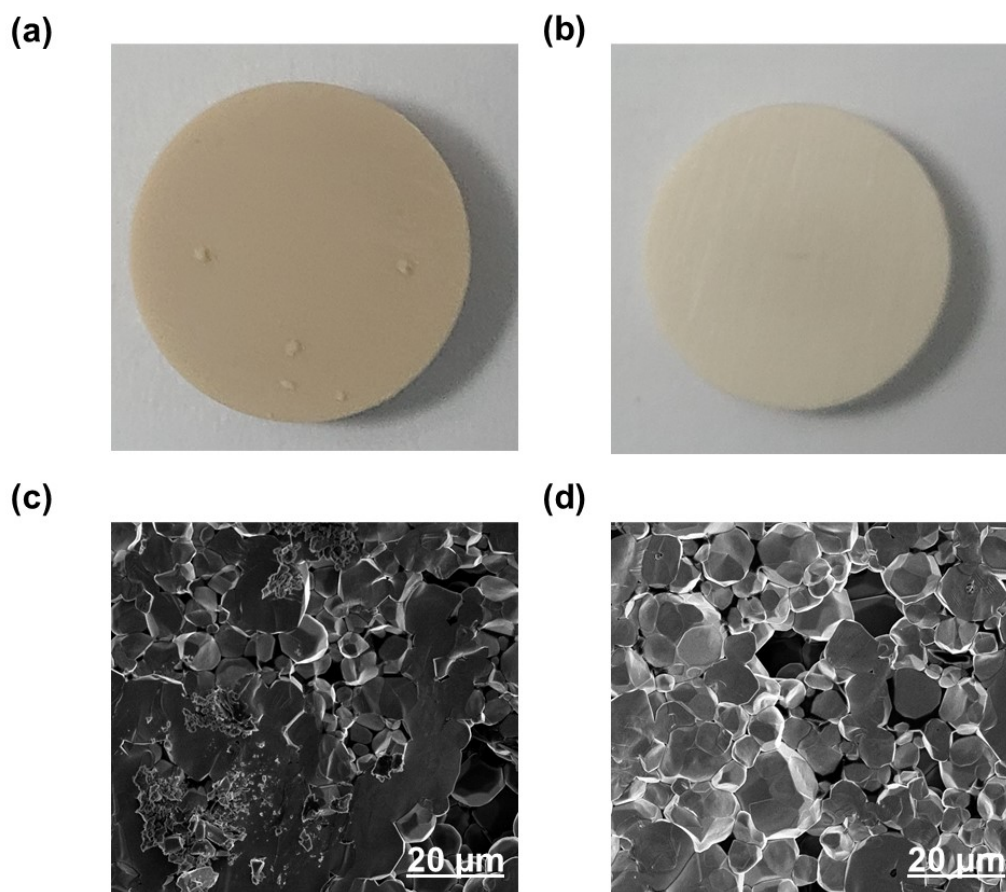


Figure S18. Images of (a) LLZTO-LZTO and (b) LLZTO ceramics sintered at 1240 °C for 0.5 h. Cross-sectional morphology of (c) LLZTO-LZTO and (d) LLZTO ceramics sintered at 1240 °C for 0.5 h.

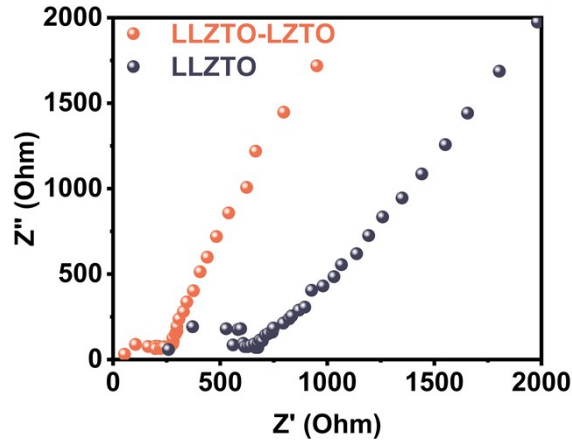


Figure S19. Impedance plots at 25 °C of LLZTO-LZTO and LLZTO SSEs.

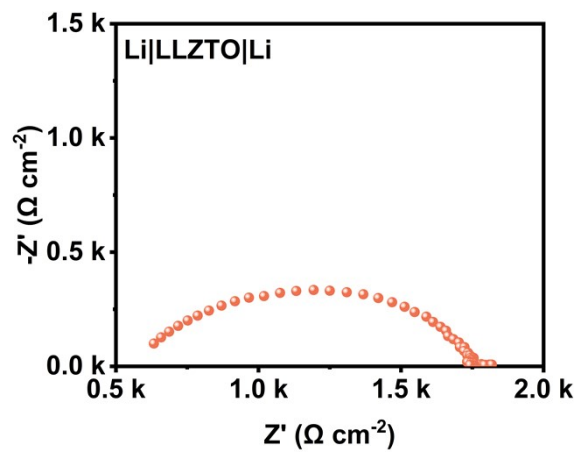


Figure S20. Nyquist plots of Li/LLZTO/Li symmetric cells at 25 °C.

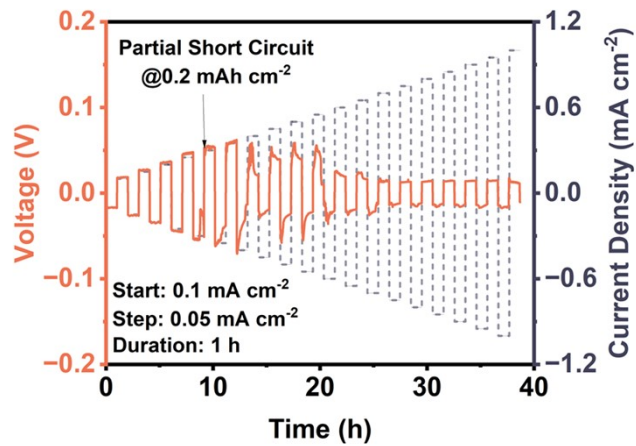


Figure S21. CCD test of Li/LLZTO/Li symmetric cells at 25 °C.

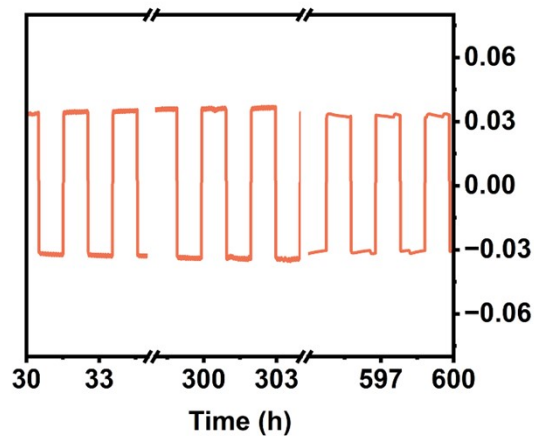


Figure S22. Cycling performance of Li|LLZTO|Li symmetric cells at 25 °C.

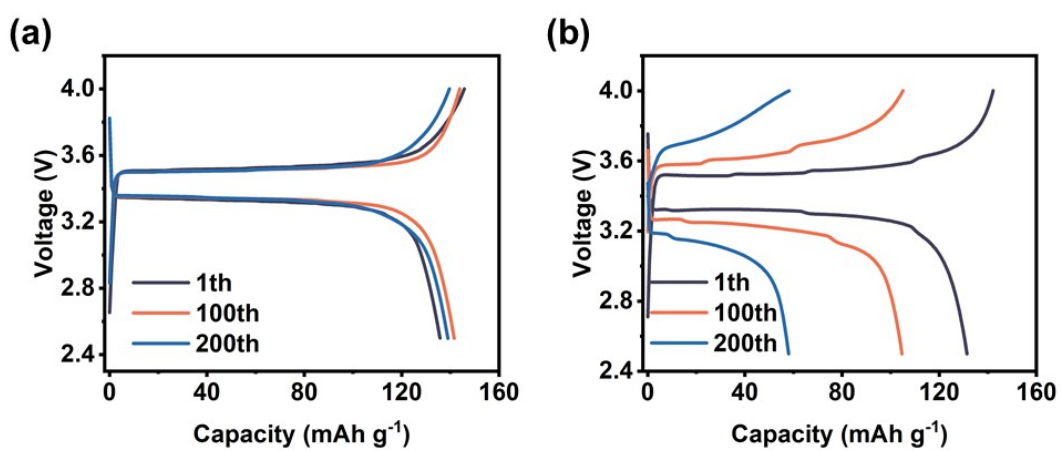


Figure S23. Charge/discharge curves for the 1st, 100th and 200th cycles of (a) LFP/LLZTO-LZTO/Li cell and (b) LFP/LLZTO/Li.

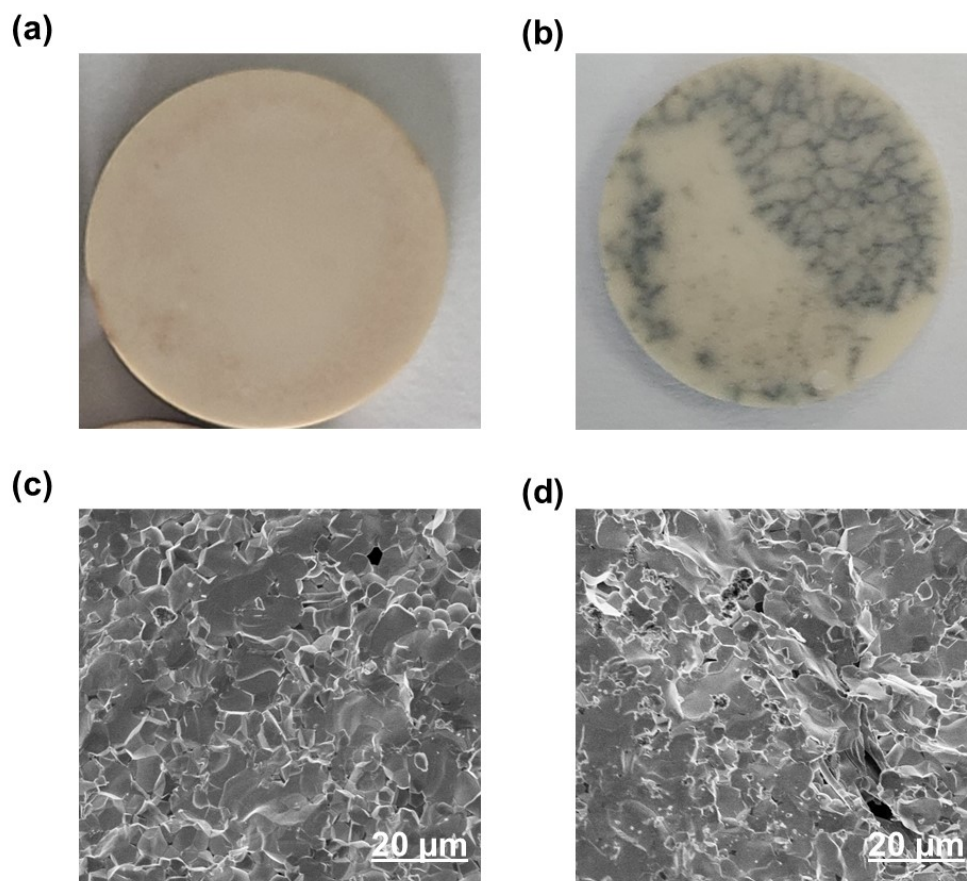


Figure S24. Images of (a) LLZTO-LZTO and (b) LLZTO ceramics sintered after cycling. Cross-sectional morphology of (c) LLZTO-LZTO and (d) LLZTO ceramics sintered after cycling.

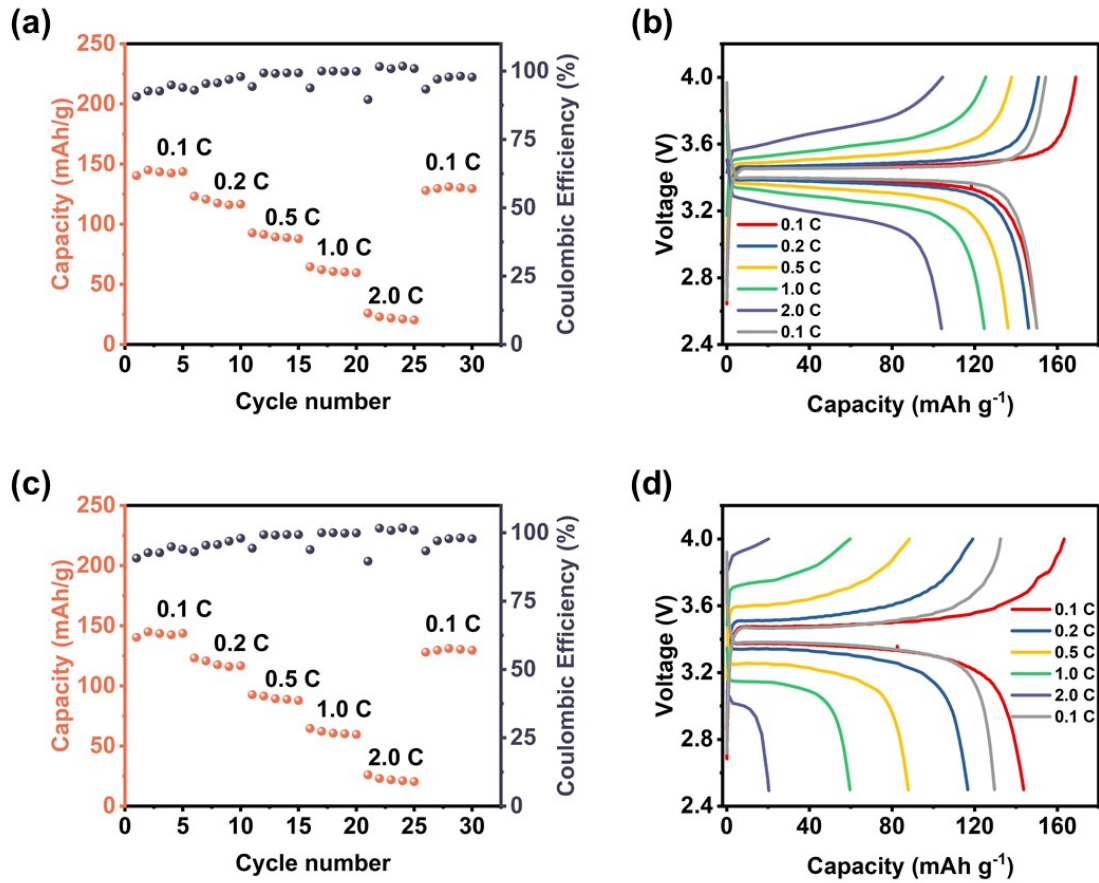


Figure S25. Rate performance of (a) Li/LLZTO-LZTO/LFP cell and (b) Li/LLZTO/LFP cell at various current densities from 0.1 to 2 C. Charge-discharge curves of (c) Li/LLZTO-LZTO/LFP cell and (d) Li/LLZTO/LFP cell from 0.1 to 2 C.

Table S1. Summary of the recycling processes of solid-state battery.

| Process | Method reported | advantage | Limitation | Reference |
|---|---|--|---|-----------|
| Deep Eutectic Solvents leaching | OXA-based DESs and LLAlZO were mixed and heated for 24 h at 80 °C. | Low temperatures, high selectivity | Low lithium recovery rate, Low solid-liquid ratio | 1 |
| Organic acid leaching | A two-step recycling approach using citric acid as the leaching agent to separate and recover the individual components of a model cell comprising NCM/LLZO/LTO. | Without strong mixing of individual phases | The elements of cathode, anode and electrolyte in the actual spent batteries are fully mixed, making it difficult to separate completely. | 2 |
| Acid Leaching-- Alkali Precipitation | The LFP/LLZO/LTO mixture was leached in two steps in HCl solutions at pH 1.0 and 0.2 and precipitated using NaOH. | strong and cost-efficient | Low recovery rate, low selectivity | 3 |
| Acid leaching | LLZO was completely dissolved in a strong acid, and hydroxides, sulfates, and oxides were used to recover various elements, respectively. | Complete separation of all elements | The process is long, complex and only at the theoretical stage. | 4 |
| Hydrometallurgical processes | Leaching of LLZTO using water, H ₂ SO ₄ , HCl, HCOOH, CH ₃ COOH, C ₂ H ₂ O ₄ and C ₆ H ₈ O ₇ . | Simple operation | Low selectivity | 5 |

Table S2. The specific costs of the entire gold recovery process.

| Total costs | Specific items | Costs (US \$ g ⁻¹ gold) | Percentage (%) |
|-----------------------------|-------------------------|------------------------------------|----------------|
| Operating costs (64.05%) | Electricity | 1970.48 | 6.43 |
| | Maintenance | 248.04 | 0.81 |
| | Labor | 10599.15 | 34.58 |
| | Depreciation | 1860.30 | 6.07 |
| | Other operating cost | 4955.65 | 16.17 |
| Capital cost (24.28%) | Equipment purchase cost | 1240.20 | 4.05 |
| | Other capital costs | 6201.01 | 20.23 |
| Material costs (11.67%) | Sulfur | 297.27 | 0.97 |
| | Sodium carbonate | 323.59 | 1.06 |
| | Oxalic acid | 129.44 | 0.42 |
| | Ethanol | 2808.18 | 9.16 |
| | Other chemicals | 19.48 | 0.06 |

Table S3. Relative density of solid electrolyte.

| | Relative Density (%) | Conductivity at 25 °C ($\times 10^{-4}$ S/cm) |
|------------|----------------------|--|
| LLZTO | 93.3 | 2.57 |
| LLZTO-LZTO | 95.1 | 6.25 |

References

1. Y. Chen, Z. Shi, X. Zhang, C. Wang, Y. Wang, Z. Niu, Y. Zhang and M. Feng, *ChemSusChem*, 2024, **18**, e202402126.
2. A. I. Waidha, A. Salihovic, M. Jacob, V. Vanita, B. Aktekin, K. Brix, K. Wissel, R. Kautenburger, J. Janek, W. Ensinger and O. Clemens, *ChemSusChem*, 2023, **16**, e202202361.
3. M. Ali Nowroozi, A. Iqbal Waidha, M. Jacob, P. A. van Aken, F. Predel, W. Ensinger and O. Clemens, *ChemistryOpen*, 2022, **11**, e202100274.
4. L. Schwich, M. Küpers, M. Finsterbusch, A. Schreiber, D. Fattakhova-Rohlfing, O.

- Guillon and B. Friedrich, *METALS-BASEL*, 2020, **10**, 1523.
5. K. Schneider, V. Kiyek, M. Finsterbusch, B. Yagmurlu and D. Goldmann, *METALS-BASEL*, 2023, **13**, 834.